Analyst

PAPER

View Article Online
View Journal

Check for updates

Cite this: DOI: 10.1039/d3an00918a

A one-tube dual-readout biosensor for detection of nucleic acids and non-nucleic acids using CRISPR-ALP tandem assay†

Xinxin Ke,[a] Yi Hu,[b] Chuanxia Chen *[c] and Tao Hu *[a]

Clustered regularly interspaced short palindromic repeats (CRISPR)-based diagnostics have been considered a next-generation molecular diagnosis tool. Single-readout mode has been extensively employed in massive CRISPR/Cas12a-based biosensors. In this work, we propose a one-tube dual-readout biosensor (CRISAT) for the first time for the detection of ultrasensitive nucleic acids and non-nucleic acids developed by harnessing CRISPR-ALP tandem assay. In the presence of a target, Cas12a is activated to randomly cut the single-stranded hyDNA sequence of MB@hyDNA-cALP, thus releasing abundant alkaline phosphatase (ALP) in the supernatant solution. By using 4-aminophenol phosphate as the substrate of ALP, *p*-aminophenol is produced, which then reacts with *N*-[3-(trimethoxysilyl)propyl]ethylenediamine or diethylenetriamine to generate silicon-containing polymer carbon dots (Si PCDs) or polymer carbon dots (PCDs) *in situ*, which can be observed by the naked eye or detected using a fluorescent device in the same solution. Using this strategy, a fluorescence and colorimetry dual-readout nanoplatform for CRISPR-based biosensors can be rationally developed. We ascertain the applicability of CRISAT by detecting the SARS-CoV-2 pseudovirus, achieving superior sensitivity and specificity. With simple modification of crRNAs, the CRISAT platform can also be employed to detect monkeypox virus (MPXV) and non-nucleic acids of adenosine triphosphate (ATP). This work shows great potential for the detection of nucleic acids and non-nucleic acids.

Received 6th June 2023,
Accepted 25th July 2023

DOI: 10.1039/d3an00918a

rsc.li/analyst

Published on 25 July 2023. Downloaded by Mahidol University on 8/16/2023 7:03:27 AM.

Introduction

The clustered regularly interspaced short palindromic repeats (CRISPR)–Cas system has garnered increased scientific interest for its application in gene editing.[1,2] Also, CRISPR/Cas technology is regarded as the most recent and ongoing diagnostic tool owing to its unique nuclease activity under the direction of a guide ribonucleic acid (crRNA) to target nucleic acids.[3–8] When a double-stranded DNA (dsDNA) or single-stranded DNA (ssDNA) activator is recognized, the representative CRISPR/Cas12a presents strong "*trans*-cleavage" activity and indiscriminately cuts any unrelated ssDNA. By taking advantage of this unique trait, CRISPR/Cas12a has been widely harnessed as a promising biosensor by cleaving the functionalized reporter DNA.[9–11] In this regard, various CRISPR-based diagnostic platforms, including colorimetry, electrochemistry, electrochemiluminescence, and chemiluminescence, have been proposed.[12–21] Although the aforementioned biosensors can provide highly sensitive, selective, fast, and convenient testing, they are only available in a single-readout mode that is not conducive to the accuracy of detection due to the influence of environmental and instrumental factors. There is an urgent demand for extending and building a novel CRISPR/Cas12a-based multiple-readout biosensor.

Dual-mode methods have recently gained research attention because they can perform cross-validating detection, reduce false negative/positive probabilities, and exhibit convincing results.[22] In this manner, several CRISPR/Cas-triggered dual-mode detection strategies have been reported. For example, by separately using two different nanomaterials as signal generators, Wang's group developed a CRISPR/Cas12a-based fluorescent/colorimetric dual-signal biosensor for the sensitive detection of estradiol and prostate-specific antigen.[23] Pu's group proposed a single-base resolution analysis biosensor with dual-mode signal output of electrochemistry and

[a]*Children's Hospital, Zhejiang University School of Medicine, National Clinical Research Center for Child Health, Hangzhou, 310052, China. E-mail: hutaozd@zju.edu.cn*
[b]*Hefei National Lab for Physical Sciences at the Microscale and the Centers for Biomedical Engineering, University of Science and Technology of China, Hefei, 230027, China*
[c]*School of Materials Science and Engineering, University of Jinan, Jinan, Shandong, 250022, China. E-mail: mse_chencx@ujn.edu.cn*

† Electronic supplementary information (ESI) available. See DOI: https://doi.org/10.1039/d3an00918a

Published on 25 July 2023. Downloaded by Mahidol University on 8/16/2023 7:03:27 AM.

fluorescence based on the CRISPR/Cas12a-triggered cleavage of various ssDNA-labeled reporters in separate reactors. Multimode detection can also be achieved by treating the same fragment solution using different strategies.[24] Ma' group established a colorimetric and photothermal dual-signal CRISPR/Cas12a-powered biosensor based on DNA-labeled gold nanoparticles by recording the color change after centrifugation and measuring the temperature change of the supernatant after laser irradiation.[25] Additionally, a dual-mode electrochemical (fast scan voltammetric and electrochemiluminescence) biosensor for the detection of genetically modified soybean SHZD32-1 was proposed.[26] In particular, the signal output of the aforementioned dual-mode detection strategies needs to provide independent probes or beacons and cannot be achieved synchronously, which may result in complicated operation steps and high costs. It is still desirable to find a simpler and more cost-effective dual-mode detection strategy for CRISPR-based biosensors.

Fluorescence and colorimetric dual-mode signals that are strictly generated from identical precursors in one tube can make detection easier and economical. Recently, by using *p*-aminophenol (AP) as a raw material, nanomaterial-based dual-mode alkaline phosphatase (ALP) assays with greatly improved detection performances have been reported, benefiting from the easy and convenient synthesis and superior fluorescence and colorimetric properties of the *in situ* generated nanomaterials.[22,27] The ALP-catalyzed signal mode implied that it could be used to establish a CRISPR-based dual-readout platform by using the collateral cleavage ability of Cas12a on ssDNA, which could indirectly or directly cut ssDNA combined with the ALP native enzyme. To the best of our knowledge, the proposed biosensor has not yet been reported.

Inspired by ALP-involved dual-signal detection, we have developed a unique CRISPR/Cas12a-ALP tandem platform (denoted as CRISAT), which utilizes the catalytic properties of ALP to generate AP and the synthesis of carbon dots (CDs) *in situ*, to realize one-tube dual-readout for the detection of target nucleic acids or non-nucleic acids. As demonstrated in Scheme 1, one terminus of hybridization DNA (hyDNA) is immobilized on the magnetic beads (MB), and the other end is capable of coupling abundant ALP with the aid of tyramide amplification (TSA) technology. After target recognition, the hyDNA on the surface of MB@hyDNA-cascade ALP (MB@hyDNA-cALP) was cleaved by the activated Cas12a, thus releasing abundant ALP in the supernatant. The free ALP further catalyzes the hydrolysis of 4-aminophenyl phosphate (APP) to generate AP, which then reacts with *N*-[3-(trimethoxysilyl)propyl]ethylenediamine (DAMO) or diethylenetriamine (DETA) precursors to generate silicon-containing polymer carbon dots (Si PCDs) or PCDs. In contrast to present dual-mode methods, this process simultaneously provides both fluorescence and absorbance signals in one tube that can be observed by the naked eye or detected using a fluorescent device. This dual-readout nanoplatform based on CRISPR/Cas12a can be applied to detect both nucleic acid and non-nucleic acid analytes. Due to its high sensitivity, visualization or use of a fluorescence tool, and simple workflow, this platform is suitable for facile point-of-care (POC) detection.

Materials and methods

Materials and apparatus

LbCas12a was bought from Guangzhou Magigen Biotechnology Co., Ltd. Streptavidin-ALP, streptavidin-HRP, and BeyoMag™ Streptavidin Magnetic Beads (MB) were obtained from Beyotime Biotechnology (Shanghai, China). Biotin-tyramine was obtained from APExBIO Technology LLC (Houston, USA). 4-Aminophenol (AP), diethanolamine (DEA), *N*-[3-(trimethoxysilyl)propyl]ethylenediamine (DAMO) and diethylenetriamine (DETA) were bought from Macklin Biochemical Co., Ltd (Shanghai, China). 4-Aminophenyl phosphate monosodium salt hydrate (APP) was obtained from Aladdin Corporation (Shanghai, China). Adenosine 5′-triphosphate disodium salt hydrate (ATP-2Na) was bought from Sigma-Aldrich (USA). Cytidine 5′-triphosphate (CTP), 5′-triphosphate (UTP), and guanosine 5′-triphosphate (GTP) were bought from Sangon Biotech (Shanghai, China). Oligonucleotides were ordered from General Biol (Anhui) Co., Ltd (Chuzhou, China), and the detailed sequences are shown in Table S1.† Pseudoviruses corresponding to SARS-CoV-2 and the monkeypox virus F3L gene were purchased from Yeasen Biotechnology (Shanghai, China). The RaPure virus RNA/DNA kit was bought from Magen (Guangzhou, China). RT-RPA and RPA kits were purchased from Jiangsu Qitian Gene Biotechnology Co., Ltd (Wuxi, China).

The transmission electron microscopy images of Si PCDs or PCDs were obtained using a Jeol JEM-1400 (80 kV, Japan). The absorbance and fluorescence data were recorded using a microplate reader (Tecan Spark GmbH, Austria).

Preparation of MB@hyDNA-ALP and MB@hyDNA-cALP

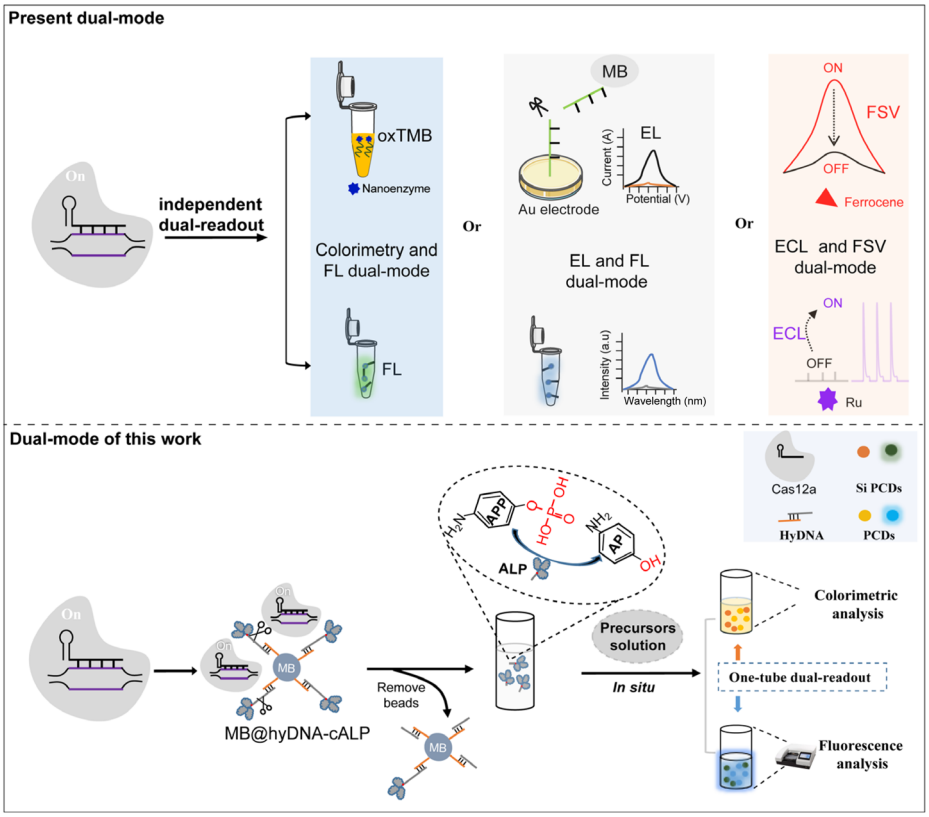
The pre-prepared MB@hyDNA and streptavidin-ALP (100 μL, 1 μg mL^{-1}) were co-incubated for 30 min to obtain MB@hyDNA-ALP. To prepare MB@hyDNA-cALP, MB@hyDNA was incubated with streptavidin-HRP (0.3 μg mL^{-1}) for 15 min. Afterwards, PBS buffer was used to wash the beads five times. After removing the supernatant, 10 μL of tyramine-ALP and 2 μL of 10 mM H_2O_2 were incubated with the beads for 10 min to form MB@hyDNA-cALP. To evaluate the effect of the TSA strategy employed in the study, MB@hyDNA-ALP and MB@hyDNA-cALP were washed using Tris-HCl buffer (20 mM, pH 8.0) five times, and 100 μL of the AMPPD substrate was incubated with beads for 90 s.

Measurement of CRISAT

The as-prepared MB@hyDNA-cALP was washed with Tris-HCl buffer (50 mM, pH 8.0, 10 mM $MgCl_2$, 150 mM NaCl) five times. After that, the supernatant was removed and 20 μL of the mixture solution containing 200 nM LbCas12a-crRNA and target nucleic acids or ATP solution was incubated with the beads for 15 min at 37 °C. The supernatant was collected by

This journal is © The Royal Society of Chemistry 2023

Published on 25 July 2023. Downloaded by Mahidol University on 8/16/2023 7:03:27 AM.



Scheme 1 Schematic diagram of the present CRISPR/Cas12a-based dual-mode biosensors *versus* the CRISPR/Cas12a-based dual-mode biosensor of this work.

separating the beads with the help of a magnetic rack. Subsequently, 2 μL of APP (3 mM), 5 μL of 1 mM $MgCl_2$, 50 μL of 50 mM Tris-HCl buffer (pH 9.8) and 145 μL of ultrapure water were added to the supernatant and incubated for 40 min at 37 °C. Finally, 75 μM DAMO or 200 μM DETA was introduced and the whole reaction solution was incubated for 20 min or 30 min at 70 °C, respectively. The absorbance and fluorescence data were recorded.

Results and discussion

In situ synthesis and characterization of Si PCDs and PCDs triggered by MB@hyDNA-cALP and *trans*-cleavage of hyDNA

In this work, we sought to use hyDNA as a bridge to couple ALP coated onto MB. We first investigated whether Cas12a is capable of cutting the single-stranded sequences of hyDNA. The sense and anti-sense strands were labeled with FAM fluorescence molecules (sequences are listed in Table S1,† Fig. 1A), and the dual-terminus labeled hyDNA was formed by 11 bases between the two single strands (Fig. 1A). A synthetic DNA (stDNA) sequence (listed in Table S1†) corresponding to the N gene of SARS-CoV-2 was used as a model target. PAGE experiments were carried out to validate the performance of the activated Cas12a, which is known to preferentially cleave A- or T-rich sequences.[28,29] As shown in Fig. 1A, lanes 1 and 2 show the FAM-labeled sense strand of hyDNA and the FAM-anti-sense strand of hyDNA, respectively. Compared to lane 3 without a target, we observed that the prepared hyDNA could be digested into short products in lane 4, which simultaneously contains Cas12a-crRNA and the stDNA target. This result demonstrated that the dual-terminus poly A sequences of hyDNA were effectively cut by Cas12a.

Thereafter, we turned our attention to exploring the performances of the as-obtained MB@hyDNA-cALP. At the beginning, only streptavidin-ALP was initially fixed onto MB@hyDNA to form MB@hyDNA-ALP. To further increase the detection sensitivity, MB@hyDNA-cALP was formed after the addition of streptavidin-HRP, tyramine-ALP, and H_2O_2, which allows the production of abundant HRP-tyramine-ALP using the classical TSA strategy; the structural difference between MB@hyDNA-cALP and MB@hyDNA-ALP is shown in Fig. S1.† Upon the addition of the AMPPD substrate of ALP, a chemiluminescence (CL) signal intensity was observed in the MB@hyDNA-ALP and MB@hyDNA-cALP groups. As expected, the CL intensity in the MB@hyDNA-cALP group was nearly three-fold higher than that in the MB@hyDNA-ALP group (Fig. 1B), indicating that the introduction of the TSA strategy improved the ability of the beads to load more ALP. Hence, we used MB@hyDNA-cALP for further experiments.

Subsequently, we studied the feasibility of the *in situ* formation of Si PCDs or PCDs induced by the MB@hyDNA-cALP.

Published on 25 July 2023. Downloaded by Mahidol University on 8/16/2023 7:03:27 AM.

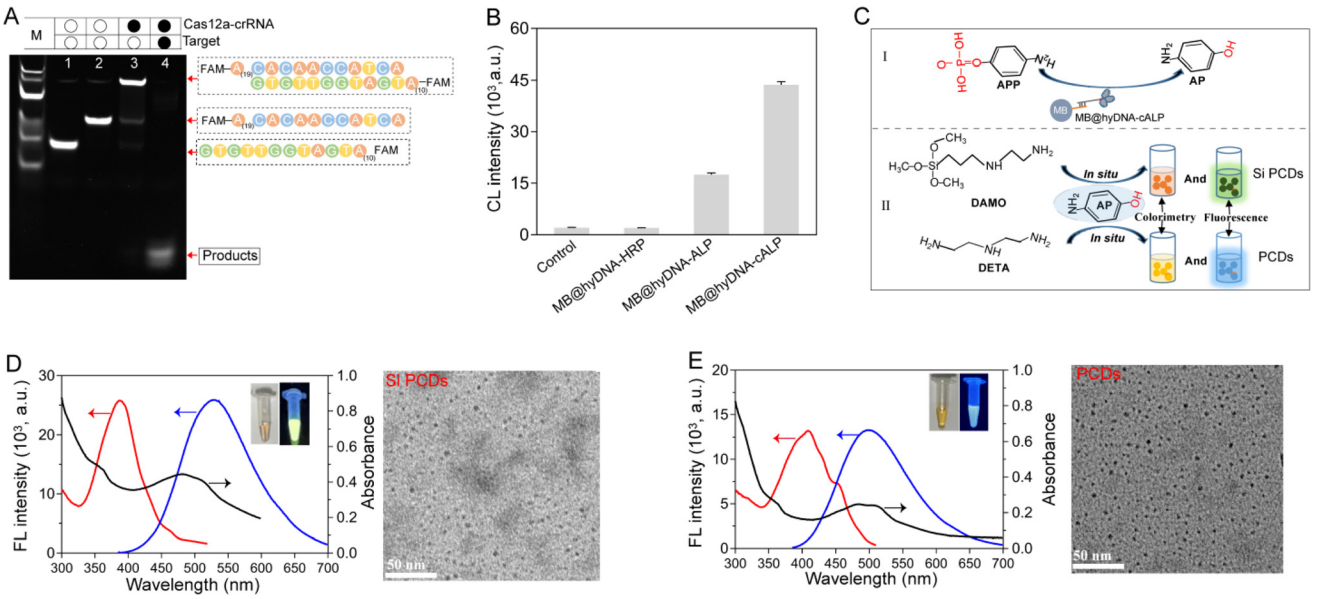


Fig. 1 (A) Native PAGE analysis of the Cas12a collateral cleavage of 400 nM hyDNA. Lane 1: Antisense strand of hyDNA, lane 2: sense strand of hyDNA, lane 3: hyDNA, and lane 4: cleaved products. (B) CL intensity of the control, MB@hyDNA-HRP, MB@hyDNA-ALP and MB@hyDNA-cALP groups. (C) Schematic representation of fluorescence and colorimetric reactions according to the *in situ* generation of Si PCDs and PCDs induced by MB@hyDNA-cALP. (D) Absorption spectrum (the black line and black arrow corresponding to the Y-line), fluorescence excitation spectrum (the red line and red arrow corresponding to the X-line), fluorescence emission spectrum (the blue line and blue arrow corresponding to the X-line) and the TEM image of Si PCDs (right panel). (E) Absorption spectrum (the black line and black arrow corresponding to the Y-line), fluorescence excitation spectrum (the red line and red arrow corresponding to the X-line), fluorescence emission spectrum (the blue line and blue arrow corresponding to the X-line) and the TEM image of PCDs (E, right panel). The insets (D and E) show the resultant solutions under white and 365 nm UV light, respectively.

The sensing principle is displayed in Fig. 1C. The MB@hyDNA-cALP catalyzes the hydrolysis of APP to produce AP, which then reacts with DAMO or DETA to generate Si PCDs or PCDs, turning orange-red or yellow under white light, respectively. While being exposed to UV light (365 nm), the solutions emit intense yellow-green and light green fluorescence, respectively (Fig. 1D and E, left inset). As shown in the transmission electron microscopy image (Fig. 1D and E, right inset; Fig. S2†), the average sizes of the generated Si PCDs and PCDs were identified to be 3.6 ± 0.03 nm and 3.28 ± 0.04 nm, respectively. Moreover, the generated Si PCDs and PCDs reveal typical absorption peaks at 483 and 480 nm, respectively (Fig. 1D and E, left inset). The fluorescence spectra of Si PCDs displayed the excitation and emission peaks at 376 nm and 524 nm, respectively, and those of PCDs were observed at 400 nm and 510 nm, respectively (Fig. 1D and E, left inset). Taken together, these results explicitly suggested that Si PCDs and PCDs *in situ* generated by MB@hyDNA-cALP possess both colorimetric and fluorescence properties.

Development of the CRISAT platform

To test the feasibility and effectiveness of the proposed platform, Cas12a's collateral cleavage activity was initially triggered after the addition of the stDNA target and Cas12a-crRNA. Thereafter, the entire mixture was incubated with MB@hyDNA-cALP, and thus the hyDNA could be cleaved indiscriminately. The obtained supernatant containing abundant ALP sequentially reacted with APP and DAMO solutions. As depicted in Fig. 2A and B, the MB@hyDNA-cALP with the stDNA group displayed intense fluorescence and colorimetric values, accompanied by yellow-green and orange-red fluorescence under UV and white light, respectively (inset pictures). In sharp contrast, the solutions of the control and MB@hyDNA-cALP were unable to emit discernible fluorescence and generate distinctive absorption peaks of Si PCDs. As for the addition of DETA, the color of the final solution was light green and yellow under UV and white light, respectively (Fig. S3A and S3B,† inset pictures). These results indicated that the proposed platform has potential for one-tube multiple-readout detection of nucleic acids.

We next optimized the experimental conditions to enhance the detection efficiency of the platform. Initially, we investigated the roles of the volume of MB and concentrations of hyDNA and streptavidin-HRP toward maximizing bead loading efficiency. The results indicated that the fluorescence signals reached their plateau levels when using 4 μL MB, 0.4 μM hyDNA and 0.3 μg mL^{-1} streptavidin-HRP (Fig. S4A–C†). Subsequently, we turned our attention to the Cas12a reaction conditions. As displayed in Fig. 2C and D, the optimum concentration and cleavage time of Cas12a were 200 nM and 15 min, respectively. We further explored the analytical performance for ALP activity. On the basis of the results illustrated in Fig. 2E and Fig. S4D,† 40 min of APP reaction time and 30 μM APP were adopted because a further increase in the

This journal is © The Royal Society of Chemistry 2023

Published on 25 July 2023. Downloaded by Mahidol University on 8/16/2023 7:03:27 AM.

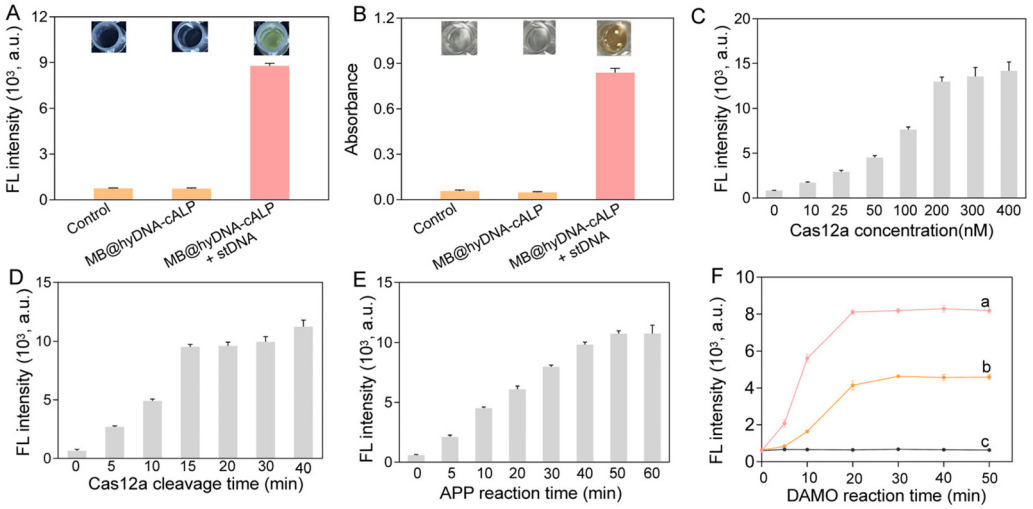


Fig. 2 Feasibility of the established CRISAT platform for fluorescence (A) and colorimetric (B) detection of the stDNA target based on Si PCDs. The insets of (A) and (B) show visual images under UV and white light, respectively. (C) Fluorescence intensity as a function of Cas12a concentration. (D) Evaluation of the effects of Cas12a cleavage time. (E) Evaluation of the effects of APP reaction time. (F) Fluorescence intensity as a function of DAMO reaction time using different stDNA concentrations: 0 nM (a), 2 nM (b), and 4 nM (c).

APP concentration and the reaction time did not enhance the fluorescence intensity. Additionally, a DAMO concentration of 75 μM (Fig. S5A†) and a reaction time of 20 min (Fig. 2F), as well as a DETA concentration of 200 μM (Fig. S5B†) and a reaction time of 30 min (Fig. S5C†) were chosen for the subsequent assay.

Analytical performance of the CRISAT platform

The sensing performance of the CRISAT platform was evaluated under optimal conditions. With an elevated concentration of stDNA, gradual increases in the fluorescence intensity and absorbance were observed (Fig. 3A and B) because of the increased concentrations of ALP caused by the gradual activity of Cas12a. Meanwhile, visible color changes were also easily discernible with the naked eye (insets in Fig. 3A and B). More to the point, Fig. 3A indicates that the fluorescence intensity exhibited a satisfactory linear correlation with the stDNA concentrations ranging from 0.1 nM to 3 nM. The regression equation can be expressed as $F_{524} = 2480\ C_{\mathrm{stDNA}}\ (\mathrm{nM}) + 219$, $R^2 = 0.998$ (Fig. 3B). Compared with the fluorescent channel, the colorimetric intensity exhibited a narrower linear range (0.1 nM–2 nM), and the regression equation between the absorbance and stDNA concentration can be expressed as $A_{480} = 0.0179\ C_{\mathrm{stDNA}}\ (\mathrm{nM}) + 0.076$, $R^2 = 0.992$ (Fig. 3B). The limits of detection (LODs) of fluorometric and colorimetric modes were estimated to be 12 pM and 42 pM ($3\sigma/S$), respectively. Similarly, both the fluorescence and colorimetric signals for PCD readout depicted a stDNA-dependent enhancement behavior (Fig. S6†), and the detection limits were also determined (23 pM for fluorescence and 48 pM for colorimetry). The detection limits of the CRISAT assay were comparable with or superior to those of most reported CRISPR-based single-readout biosensor assays (Table S2†).

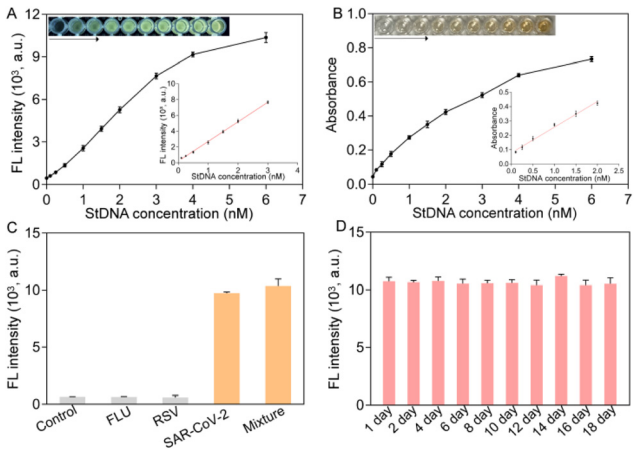


Fig. 3 (A) Fluorescence intensity as a function of stDNA concentrations (0, 0.1, 0.25, 0.5, 1, 1.5, 2, 3, 4, and 6 nM) based on Si PCDs (top inset: visual photo changes with the increase of stDNA concentration under 365 nm UV light; right inset: calibration curve over the range of 0.1–3 nM). (B) Absorbance intensity as a function of stDNA concentrations (0, 0.1, 0.25, 0.5, 1, 1.5, 2, 3, 4, and 6 nM) based on Si PCDs (top inset: visual photo changes with the increase of stDNA concentration under natural light; right inset: a calibration curve over the range of 0.1–2 nM). (C) Specificity of the CRISAT platform for SARS-CoV-2 by comparison with FLU and respiratory syncytial virus (RSV). (D) Evaluation of the stability of the CRISAT platform.

The specificity of the platform was verified by using stDNAs corresponding to influenza B (FLU), respiratory syncytial virus (RSV) and SARS-CoV-2. As shown in Fig. 3C, the fluorescence intensities of the FLU and RSV groups were similar to that of the control group. In striking contrast, the fluorescence intensity for SARS-CoV-2 and the mixed groups markedly increased, suggesting that the designed crRNA was specific for SARS-CoV-2 and demonstrating the higher specificity of the

Published on 25 July 2023. Downloaded by Mahidol University on 8/16/2023 7:03:27 AM.

CRISAT platform. To investigate the stability of the platform, we focused on the preservation conditions of the as-prepared MB@hyDNA-cALP for 18 consecutive days. Derived from Fig. 3D, the values of fluorescence intensity were nearly steady with a relative standard deviation (RSD) of 3.09%, indicating the high stability of the CRISAT platform for nucleic acid detection.

Validation with pseudovirus samples

To test the analytical performance using real samples, the working principle of the platform is summarized in Fig. 4A. RT-RPA was employed to quickly amplify the nucleic acids of the sample, and the amplified products were mixed with Cas12a-crRNA and MB@hyDNA-cALP in a tube. After the CRISPR reaction, a supernatant containing abundant ALP was obtained. The supernatant was reacted with APP and further reacted with DAMO or DETA, which can be directly recognized by the naked eye under white light or UV light, realizing multiple-readout results. The applicability of the platform was investigated using a SARS-CoV-2 pseudovirus. The primers designed for RT-RPA are shown in Fig. 4B and the amplified products of the extracted RNA were verified by agarose gel electrophoresis (Fig. S7†). With the aid of the RT-RPA kit, the CRISAT platform could detect as few as two copies per reaction for Si PCD readout (Fig. 4C and D). The results suggested that the platform may provide a new method for the multiple-readout sensing of nucleic acids. To make the CRISAT platform more user-friendly and convenient, the reagents were assembled into four tubes; this procedure paved the way for the development of a nucleic acid detection kit (Fig. 4E).

Programmable applications of the CRISAT platform

The global spread of the monkeypox virus (MPXV) has created a global public health challenge.[30] As with COVID-19, the current assay for MPXV detection is based on the polymerase chain reaction (PCR), which requires laboratory-based testing instruments and trained experts, limiting its application in POC testing and resource-limited areas.[31] It is very simple and convenient to construct an MPXV diagnostic assay based on the CRISAT platform, by slightly changing the crRNA sequence. The MPXV-related crRNA and RPA primers were designed (Fig. 5A, sequences are listed in Table S1†) based on the F3L genome, where the performance of primers has been evaluated by agarose gel electrophoresis of amplification bands (Fig. S7†). As shown in Fig. 5B and C, using Si PCD readout as an example, we found that the CRISAT platform could detect as few as two copies per reaction in the MPXV pseudotype virus sample with the help of the RPA kit, highlighting its significant practicability for MPXV diagnosis. Additionally, the method is simple, has no need for expensive

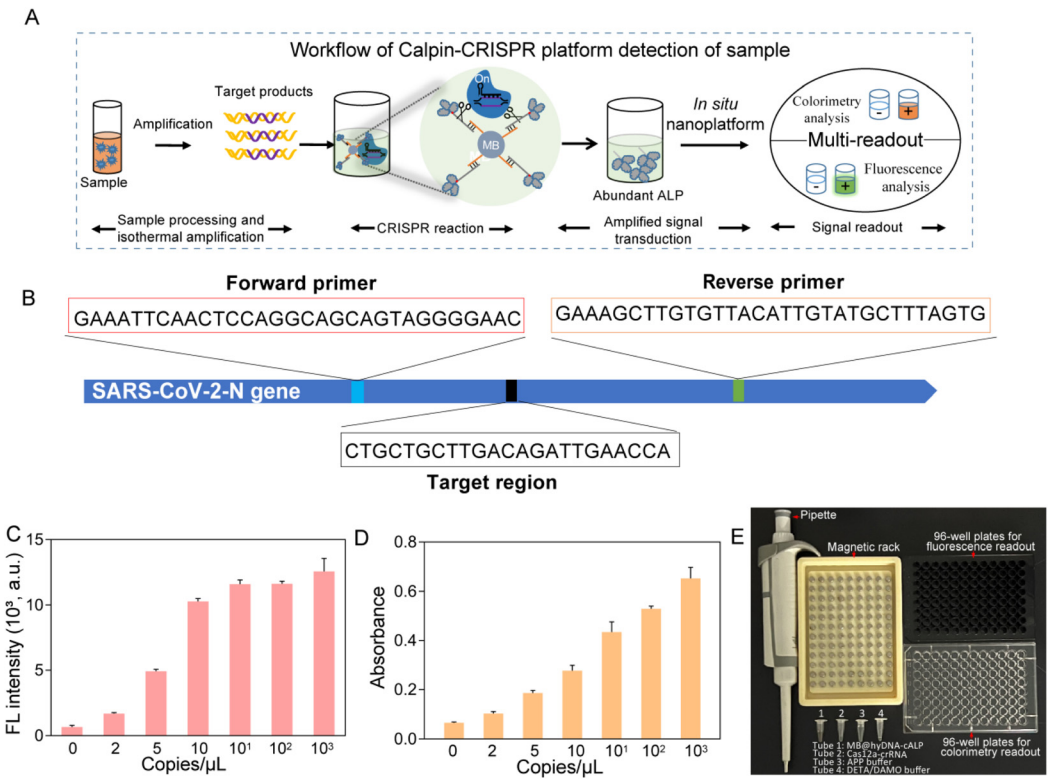


Fig. 4 (A) Workflow of the CRISAT platform for pseudovirus sample detection. (B) Schematic of the SARS-CoV-2-N gene and the targeted sequences used to design RPA primers. (C) Fluorescence channel evaluation of the sensitivity detection of SARS-CoV-2 by combining the RPA kit. (D) Colorimetry channel evaluation of the sensitivity detection of SARS-CoV-2 by combining the RPA kit. (E) Main laboratory equipment and assembled reagents needed for the CRISAT assay.

 This journal is © The Royal Society of Chemistry 2023

Published on 25 July 2023. Downloaded by Mahidol University on 8/16/2023 7:03:27 AM.

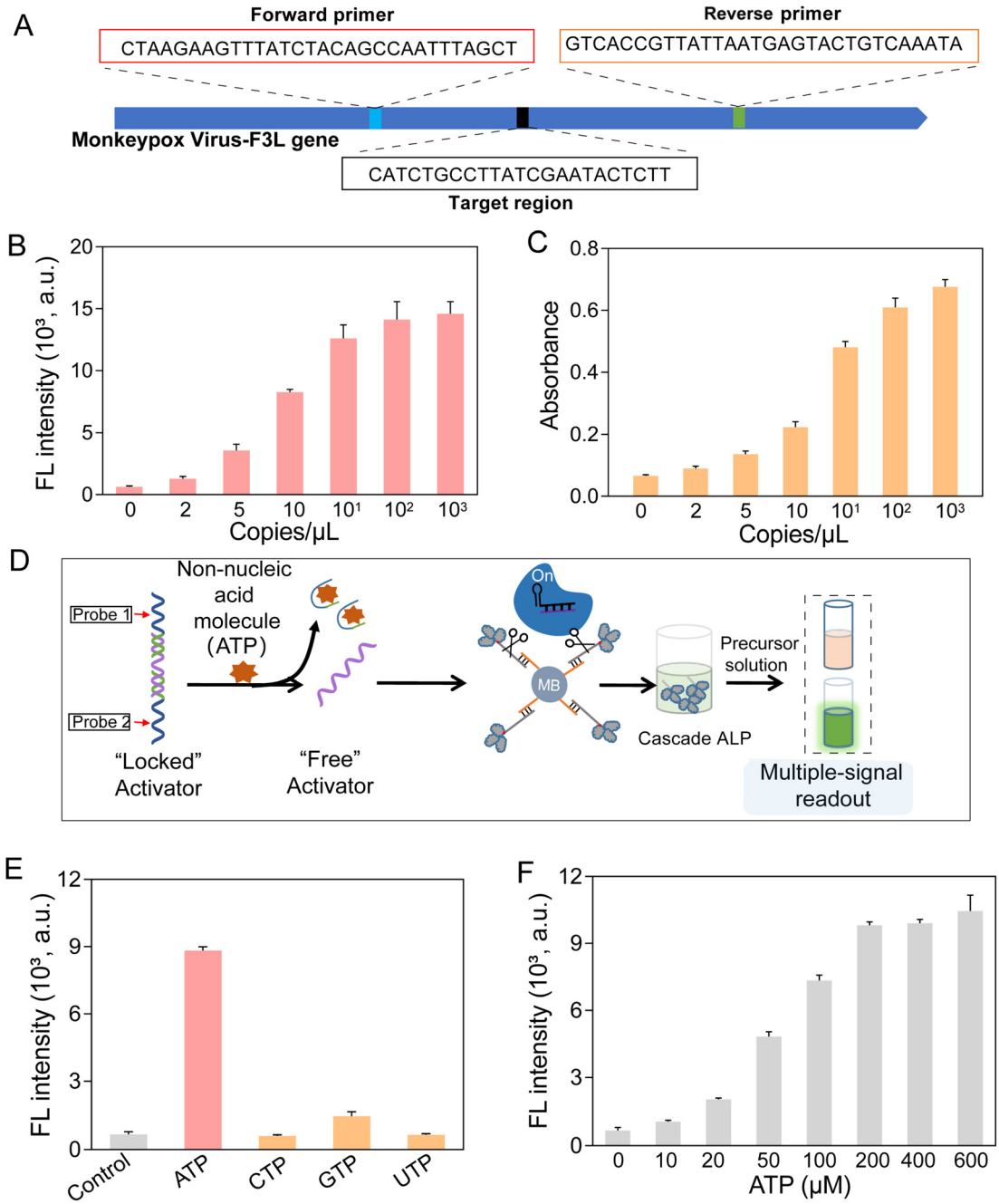


Fig. 5 (A) Schematic of the monkeypox virus-F3L gene and targeted sequences used to design RPA primers. (B) and (C) Sensitivity detection of the monkeypox virus-F3L gene by combining the RPA kit. (D) Workflow of CRISAT for detecting non-nucleic acid molecules (*e.g.*, ATP). (E) Specificity evaluation of CRISAT for detecting ATP using its analogues. (F) Sensitivity evaluation of the CRISAT platform for ATP.

equipment, and is time-efficient in comparison with the standard qPCR method.

Finally, we further extended the application of the CRISAT platform for detecting target non-nucleic acids by integrating LbCas12a-crRNA with an aptamer as the recognition element. The adenosine triphosphate (ATP) aptamer, which is one of the most widely utilized aptamers, has been thoroughly examined for its sequence, structure, and functionality. Moreover, the level of ATP can be employed as an indicator for cell viability and environmental analysis.[32] Here, the target activator is locked by two ATP aptamer DNA molecules denoted as "probe 1" and "probe 2" (Fig. 5D), and the detailed sequences and structures are shown in Fig. S8.† In the absence of ATP, the DNA/DNA hybridization of probe 1 and probe 2 with an activator shows higher thermodynamic stability than the DNA/RNA hybridization between crRNA and the single-stranded activator, preventing it from binding to the Cas12a-crRNA complex. In the presence of ATP, probe 1 and probe 2 would bind ATP

Published on 25 July 2023. Downloaded by Mahidol University on 8/16/2023 7:03:27 AM.

due to their stronger binding affinity than base complementarity, producing a free activator. As a consequence, the *trans*-cleavage activity of LbCas12a can be activated, ensuring that the CRISAT platform is feasible for ATP detection with multiple readouts. As shown in Fig. 5E, this strategy exhibited outstanding selectivity for ATP analytes since the control, CTP, GTP, and TTP groups failed to provide any response signals. Furthermore, the fluorescence intensity gradually increased with the rising ATP concentrations (Fig. 5F), and the CRISAT platform was capable of detecting as few as 10 μM of ATP. The developed platform displayed better performance than previously described biosensors using the same aptamer (Table S2†).

Conclusions

In short, a tandem CRISPR/Cas12a-ALP triggered one-tube dual-readout biosensor was developed for the first time. The combination of target-induced Cas12a activation and the subsequent release of ample ALP enabled the successful construction of dual-readout in the same tube, achieving an ultrasensitive detection of nucleic acid and non-nucleic acid targets. More significantly, the proposed CRISAT platform shows superior specificity for SARS-CoV-2 and MPXV pseudoviruses and may provide an efficient detection tool for virus induced pandemics globally. We further expanded the scope by slight modification of crRNAs and the design of appropriate aptamers and the corresponding blocking strands for the detection of ATP, and the LOD was as low as 10 μM. Although the CRISAT platform currently has limitations such as a relatively long detection time and a lack of full integration into a one-step detection process, as a proof-of-concept, this platform may pave the way to further broaden the POC applications that exhibit good potential, particularly, in the aspect of naked-eye and low-cost detection. Taken together, we deem that the CRISAT platform is expected to be applied for universal on-site analysis of nucleic acids and non-nucleic acids and encourage the development of future generations of CRISPR/Cas-based multi-readout biosensors.

Author contributions

Xinxin Ke: conceptualization, data curation, software, characterization, and writing – review & editing. Yi Hu: characterization and resources. Chuanxia Chen: writing – review & editing and conceptualization. Tao Hu: characterization and resources.

Conflicts of interest

The authors declare that they have no known competing financial interests or personal relationships that could have appeared to influence the work reported in this paper.

Acknowledgements

This work was supported by the National Natural Science Foundation of China (21904048), the Natural Science Foundation of Zhejiang Province of China (No. LQ23H200005) and the Project of Children's Hospital Affiliated to Zhejiang University School of Medicine (Y021026).

References

1 P. Liu, K. Luk, M. Shin, F. Idrizi, S. Kwok, B. Roscoe, E. Mintzer, S. Suresh, K. Morrison, J.-B. Frazão, M.-F. Bolukbasi, K. Ponnienselvan, J. Luban, L.-J. Zhu, N.-D. Lawson and S.-A. Wolfe, *Nucleic Acids Res.*, 2019, **47**, 4169–4180.
2 R. Barrangou, C. Fremaux, H. Deveau, M. Richards, P. Boyaval, S. Moineau, D.-A. Romero and P. Horvath, *Science*, 2007, **315**, 1709–1712.
3 S.-Y. Li, Q.-X. Cheng, J.-K. Liu, X.-Q. Nie, G.-P. Zhao and J. Wang, *Cell Res.*, 2018, **28**, 491–493.
4 D.-C. Swarts and M. Jinek, *Mol. Cell.*, 2019, **73**, 589–600.
5 Y. Wang, Y. Zhang, J. Chen, M. Wang, T. Zhang, W. Luo, Y. Li, Y. Wu, B. Zeng, K. Zhang, R. Deng and W. Li, *Anal. Chem.*, 2021, **93**, 3393–3402.
6 Z. Xu, D. Chen, T. Li, J. Yan, J. Zhu, T. He, R. Hu, Y. Li, Y. Yang and M. Liu, *Nat. Commun.*, 2022, **13**, 6480.
7 L. Ding, Y. Wu, L.-E. Liu, L. He, S. Yu, C.-Y. Effah, X. Liu, L. Qu and Y. Wu, *Biosens. Bioelectron.*, 2022, **219**, 114827.
8 M. Duan, B. Li, Y. Zhao, Y. Liu, Y. Liu, R. Dai, X. Li and F. Jia, *Biosens. Bioelectron.*, 2022, **219**, 114823.
9 X. Ding, K. Yin, Z. Li, R. V. Lalla, E. Ballesteros, M.-M. Sfei and C. Liu, *Nat. Commun.*, 2020, **11**, 4711.
10 L. Wu, X. Wang, X. Wu, S. Xu, M. Liu, X. Cao, T. Tang, X. Huang and H. Huang, *ACS Appl. Mater. Interfaces*, 2022, **14**, 50534–50542.
11 R. Nouri, Z. Tang, M. Dong, T. Liu, A. Kshirsagar and W. Guan, *Biosens. Bioelectron.*, 2021, **178**, 113012.
12 N. Mohammad, S.-S. Katkam and Q. Wei, *Angew. Chem., Int. Ed.*, 2022, **61**, e202213920.
13 Y. Dai, R.-A. Somoza, L. Wang, J.-F. Welter, Y. Li, A.-I. Caplan and C.-C. Liu, *Angew. Chem., Int. Ed.*, 2019, **58**, 17399–17405.
14 Y. Jiang, M. Hu, A.-A. Liu, Y. Lin, L. Liu, B. Yu, X. Zhou and D.-W. Pang, *ACS Sens.*, 2021, **6**, 1086–1093.
15 L. Wei, Z. Wang, J. Wang, X. Wang and Y. Chen, *Anal. Chim. Acta*, 2022, **1230**, 340357.
16 C.-Y. Li, B. Zheng, L.-L. Lu, W.-K. Fang, M.-Q. Zheng, J.-L. Gao, L. Yuheng, D.-W. Pang and H.-W. Tang, *Anal. Chem.*, 2021, **93**, 12514–12523.
17 X. Ke, Y. Ou, Y. Lin and T. Hu, *Biosens. Bioelectron.*, 2022, **212**, 114428.
18 Q. Wang, Z. Zhang, L. Zhang, Y. Liu, L. Xie, S.-G. Ge and J. Yu, *ACS Appl. Mater. Interfaces*, 2022, **14**, 32960–32969.

 This journal is © The Royal Society of Chemistry 2023

Published on 25 July 2023. Downloaded by Mahidol University on 8/16/2023 7:03:27 AM.

19 O. Mukama, J. Wu, Z. Li, Q. Liang, Z. Yi, X. Lu, Y. Liu, Y. Liu, M. Hussain, G.-G. Makafe, J. Liu, N. Xu and L. Zeng, *Biosens. Bioelectron.*, 2020, **159**, 112143.
20 Q. Zhao, B. Pan, W. Long, Y. Pan, D. Zhou, X. Luan, B. He, Y. Wang and Y. Song, *Nano Lett.*, 2022, **22**, 9714–9722.
21 Q. Zhao, Y. Pan, X. Luan, Y. Gao, X. Zhao, Y. Liu, Y. Wang and Y. Song, *Biosens. Bioelectron.*, 2021, **190**, 113450.
22 C. Chen, D. Zhao, B. Wang, P. Ni, Y. Jiang, C. Zhang, F. Yang, Y. Lu and J. Sun, *Anal. Chem.*, 2020, **92**, 4639–4646.
23 Y. Wang, Y. Peng, S. Li, D. Han, S. Ren, K. Qin, H. Zhou, T. Han and Z. Gao, *J. Hazard. Mater.*, 2023, **449**, 131044.
24 Q. Pu, Y. Ye, J. Hu, C. Xie, X. Zhou, H. Yu, F. Liao, S. Jiang, L. Jiang, G. Xie and W. Chen, *Talanta*, 2023, **252**, 123754.
25 L. Ma, L. Peng, L. Yin, G. Liu and S. Man, *ACS Sens.*, 2021, **6**, 2920–2927.
26 H. Ge, X. Wang, J. Xu, H. Lin, H. Zhou, T. Hao, Y. Wu and Z. Guo, *Anal. Chem.*, 2021, **93**, 14885–14891.
27 J. An, Y. Hu, G. Liu, M. Chen, R. Chen, Y. Lyu, M. Yuan, M. Luo and Y. Liu, *J. Mater. Chem. B*, 2021, **9**, 2998–3004.
28 J.-S. Chen, E. Ma, L.-B. Harrington, M. Da Costa, X. Tian, J.-M. Palefsky and J.-A. Doudna, *Science*, 2018, **360**, 436–439.
29 D. Samanta, S.-B. Ebrahimi, N. Ramani and C.-A. Mirkin, *J. Am. Chem. Soc.*, 2022, **144**, 16310–16315.
30 J. Cohen, *Science*, 2022, **376**, 902–903.
31 M. Altindis, E. Puca and L. Shapo, *Travel Med. Infect. Dis.*, 2022, **50**, 102459.
32 X. Li, X. Chen, M. Mao, C. Peng and Z. Wang, *Biosens. Bioelectron.*, 2022, **217**, 114725.